Journal of Alloys and Compounds 871 (2021) 159474

Contents lists available at ScienceDirect

Journal of Alloys and Compounds

journal homepage: www.elsevier.com/locate/jalcom

Kinetic study of a solid-state reaction in Ag/Al multilayer thin films by *in situ* electron diffraction and simultaneous thermal analysis

Sergey M. Zharkov[a,b,*], Roman R. Altunin[a], Vladimir V. Yumashev[c], Evgeny T. Moiseenko[a], Oleg V. Belousov[a,c], Leonid A. Solovyov[c], Mikhail N. Volochaev[b,d], Galina M. Zeer[a]

[a] Siberian Federal University, 79 Svobodny pr., Krasnoyarsk 660041, Russia
[b] Kirensky Institute of Physics, Federal Research Center KSC SB RAS, Akademgorodok 50/38, Krasnoyarsk 660036, Russia
[c] Institute of Chemistry and Chemical Technology, Federal Research Center KSC SB RAS, Akademgorodok 50/24, Krasnoyarsk, 660036, Russia
[d] Reshetnev Siberian State University of Science and Technology, Krasnoyarskij rabochij 31, Krasnoyarsk 660037, Russia

ARTICLE INFO

Article history:
Received 31 October 2020
Received in revised form 15 February 2021
Accepted 9 March 2021
Available online 13 March 2021

Keywords:
Thin films
Intermetallic compound
Solid-state reaction
Phase transformations
Kinetic model
Activation energy

ABSTRACT

A solid-state reaction process in Ag/Al multilayer thin films has been investigated by the methods of *in situ* electron diffraction, simultaneous thermal analysis, transmission electron microscopy and X-ray diffraction with the aim of studying the phase formation kinetics of intermetallic compounds. The sequence of the phase transformations in the solid-state reaction has been established: Ag+Al→(Ag)+(Al)→(Ag)+δ-Ag_2Al→μ-Ag_3Al. The process of the solid-state interaction has been shown to consist of two steps; each of them is described by a kinetic model of the n^{th} order reactions with autocatalysis. The kinetic parameters of the autocatalytic process of the phase formation for δ-Ag_2Al and μ-Ag_3Al, have been determined, in particular, their apparent activation energy: 126 kJ/mol and 106 kJ/mol, respectively.

1. Introduction

Thin films based on silver and aluminum have actively been used in various areas: *e.g.* in nanophotonics: small amounts of aluminium (of about 1–2 at%) added into silver decrease the surface roughness without increasing the optical loss [1,2]; in creating organic light emitting diodes [3–5] and in the development of solar cells [6–8]. A possibility is considered of using silver and aluminium for micro- and nanojoining by solid-state bonding [9,10].

According to the equilibrium phase diagram [11] in the Ag-Al system one can experimentally observe three intermetallic phases: hcp δ-Ag_2Al (also known as the ξ-phase [12] and γ-phase [13]), a low-temperature cubic phase μ-Ag_3Al (stable at T < 450 °C) with the β-Mn structure and a high temperature phase, bcc β-Ag_3Al (stable at T > 603 °C). The existence of metastable phases is also assumed which has been predicted theoretically based on the first-principles calculations [14], for example, of the ordered hcp Ag_2Al and AgAl, Ag_5Al *etc.*, however, at present, the existence of these phases has not been confirmed experimentally.

In [15,16] experimental investigations of the intermetallic compound formation were carried out and their mechanical properties at the interface between Ag and Al were studied. It was revealed that the μ-Ag_3Al phase had considerably higher hardness and lower fracture toughness as compared to the δ-Ag_2Al phase. Also, it was demonstrated that μ-Ag_3Al had the fracture characteristics of brittle materials. As to δ-Ag_2Al, it could endure plastic deformation prior to fracture. It was shown in [15–19], that in the case of the presence of the μ-Ag_3Al phase the destruction of the Ag/Al bond often occurred in the area of the presence of this phase because of its low fracture toughness and low corrosion resistance, thus, it is desirable to avoid the formation of the μ-Ag_3Al phase in the process of bonding. There was also some research which showed that in order to inhibit the formation of μ-Ag_3Al, dopants, such as Pd [17], Pd-Au [18], In [19] could be used.

One of the most promising directions is to use a reactive multilayer thin film to join heterogeneous materials [20,21]. In [22] the influence of the bilayer thickness on the phase formation and diffusion kinetics was studied in the multilayer Ag/Al films in the solid-state reaction process between the nanolayer of silver and aluminium (namely, the influence of the bilayer thickness in the

* Corresponding author at: Siberian Federal University, 79 Svobodny pr., Krasnoyarsk 660041, Russia.
E-mail address: zharkov@iph.krasn.ru (S.M. Zharkov).

https://doi.org/10.1016/j.jallcom.2021.159474
0925-8388/

multilayer films with the atomic ratio Ag:Al=2:1 and the total thickness of 4 μm). It was established that the apparent activation energy of the δ-Ag_2Al phase formation in the case of the Ag/Al bilayer thickness of 10 nm, was equal to 103 kJ/mol; in the case of increasing the bilayer thickness to 100–400 nm the activation energy increased to 111–125 kJ/mol. In [23] it was reported that the apparent activation energy of the δ-Ag_2Al phase formation in the Ag/Al bilayer films with the thickness of 300–700 nm was equal to 110 kJ/mol. In [24] it was observed that the effective activation energy of the δ-Ag_2Al phase in the case of its formation in the Ag/Al bilayer films with the thickness of 460 nm was equal to 83 kJ/mol. Thus, there are few studies [22–24], where the activation energy of the δ-Ag_2Al phase formation is determined, with the phase being formed in the solid-state reaction between the silver and aluminium nanolayers and the data are not always in agreement. However, there is no information concerning the activation energy of the μ-Ag_3Al phase formation.

In our previous paper [25] it was shown that, in the course of the reaction between the Al and Ag nanolayers, the δ-Ag_2Al intermetallic compound was the first one to be formed and then μ-Ag_3Al phase started to form. So, to determine the kinetic parameters of the phase formation processes for the δ-Ag_2Al and μ-Ag_3Al phases in the solid-state reaction in the Ag/Al multilayer thin films it is necessary to choose the atomic proportion of Ag and Al which provides the formation of the μ-Ag_3Al phase. According to the phase equilibrium diagram [12] the stability area of the low temperature phase μ-Ag_3Al is located in the aluminium concentration range from 21 to 25 at%. However, at such concentrations, a small amount of the δ-Ag_2Al phase can also be present as the final product of solid-state reaction along with the μ-Ag_3Al phase. Moreover, at the aluminium concentrations lower than 21 at% only the μ-Ag_3Al phase and solid solution based on silver (Ag) will be observed as the final products of the reaction.

2. Materials and methods

Ag/Al multilayer thin films were obtained by the successive deposition of aluminium and silver nanolayers with the help of pulse direct current (DC) magnetron sputtering (100 kHz). The 2 in. diameter circular sputter sources (ONYX, Angstrom Sciences) were used. The basic residual pressure was 1×10^{-4} Pa and the argon pressure during sputtering was 0.26 Pa. The high-purity materials (Girmet Ltd.) Ag (99.99 wt%) and Al (99.999 wt%) were used as the targets. The film thickness was controlled using a Bal-Tec QSG-100 quartz crystal thickness monitor. The deposition rate of Ag was 0.86 nm/s, that of Al being 0.40 nm/s. Ag/Al bilayer thin films were obtained to conduct *in situ* electron diffraction and transmission electron microscopy (TEM) experiments. TEM grids (Ted Pella Inc.) coated with a thin amorphous carbon layer with a thickness ~5 nm were used as the substrate for the bilayer film deposition. The thicknesses of the silver and aluminium nanolayers were chosen in order to have the silver concentration of 80 at% and the aluminium concentration of 20 at%. As a result, the thickness of the silver layer was ≈80 nm, that of aluminium was ≈20 nm, with the total thickness of Ag/Al bilayer ≈100 nm. In the case of the Ag/Al bilayer films the upper layer was Ag, the sequence was chosen to protect the Al nanolayer from oxidation. For obtaining reliable data when carrying out investigations by the method of simultaneous thermal analysis (STA) it is necessary to have a significant portion of the material (about 20–30 mg), for this purpose $(Ag/Al)_{15}$, multilayer films were obtained consisting of 15 bilayers of Ag/Al. The thickness of the individual layers, similar to the bilayer films, was equal to: Ag ≈80 nm, Al ≈20 nm. Thus, the total thickness of the $(Ag/Al)_{15}$ film was ≈1.5 μm. Glass substrates were used for the $(Ag/Al)_{15}$ film deposition. The substrate temperature during the deposition was equal to room temperature (25 °C).

The investigations of the microstructure, phase and elemental composition of the Ag/Al multilayer films were carried out by the methods of transmission electron microscopy (TEM), selected area electron diffraction (SAED), and energy-dispersive spectroscopy (EDS) using a high resolution transmission electron microscope JEOL JEM-2100 at an accelerating voltage 200 kV. The SAED patterns were obtained from an area of the film with the diameter of 1.3 μm.

The elemental composition of the multilayer films was studied using a JEOL JSM-7001 F scanning electron microscope equipped with an Oxford Inca Energy 350. The elemental compositions of the investigated films were: Ag = 80.0 ± 0.5 at%, Al = 20.0 ± 0.5 at%.

The films deposited on the TEM grids were heated directly in the JEOL JEM-2100 column (the pressure being 1×10^{-6} Pa) using a heating sample holder (Gatan Model 652 Double Tilt Heating Holder). The film was heated from room temperature to 300 °C, experiments at different heating rates were carried out: 5 °C/min or 10 °C/min. During continuous heating, the electron diffraction patterns were recorded by a Gatan UltraScan 1000 CCD camera at a rate of 5 or 10 frames per minute, in accordance with the heating rate (5 °C/min or 10 °C/min). So, the recorded neighboring patterns corresponded to the changes in the sample temperature equal to 1 °C. The exposure time of recording the electron diffraction pattern was equal to 1 s, thus the change in the sample temperature during the recording of one pattern was not more than 0.2 °C. The obtained sequence of the electron diffraction patterns during the sample heating allows one to establish the temperature and sequence of the phase formation during the solid-state reaction between the nanolayers. The accuracy of determining the lattice spacing with the help of electron diffraction was better than ±0.5% and the electron diffraction patterns were interpreted using the software DigitalMicrograph (Gatan) and the databases ICDD PDF 4 + [26] and Pearson's Crystal Data [27]. The authors successfully used this method to investigate the process of solid-state reaction in a variety of thin film nanosystems: Al/Cu [28,29], Al/Pt [30], Al/Ag [25], Cu/Au [31], Al/Fe [32], Fe/Si [33], Fe/Pd [31,34,35].

Cross-section specimens for the investigation by transmission electron microscopy were prepared by a focused ion beam (FIB) using a Hitachi FB-2100 (40 kV accelerating voltage) with the subsequent Ar^+ polishing at 0.5 kV.

Powder X-ray diffraction (XRD) data were collected at 25 °C using a PANalytical X'Pert PRO diffractometer operating with the CuK_a radiation (1.541874 Å) in the scan range from 10° to 100° 2θ (step width = 0.02° 2θ; time per step 10 s).

The simultaneous thermal analysis (STA) including thermogravimetry (TG) and differential thermal analysis (DTA) of the $(Ag/Al)_{15}$ multilayer samples was carried out using a simultaneous thermal analyzer Jupiter STA 449 C ("Netzsch", Germany) in Pt-Rh crucibles with perforated lids. To provide full contact the fragments of the sample film had preliminary been pressed into pellets with a diameter of 6 mm and weight of 19.4 ± 0.2 mg at a pressure of 70.7 MPa for 3 min. The simultaneous recording of the mass change (by the method of thermogravimetry), and of the heat flow (by the method of differential thermal analysis) were carried out in the range of 40–300 °C at different heating rates –5, 10 and 20 °C/min in a dynamic argon atmosphere (with the purity of 99.999%) and at the total flow rate of 50 cm^3 STP/min. For processing the preliminary thermoanalytical data, the licensed software NETZSCH Proteus ver.4.8.4. was used. The kinetic parameters of the phase formation were calculated using the software package NETZSCH Thermokinetics 3 ver.2006.08.

3. Results and discussions

3.1. Structural properties (TEM, electron and X-ray diffraction)

Fig. 1(a) presents the TEM image obtained from the Ag/Al bilayer film at the initial state. The size of the aluminium and silver

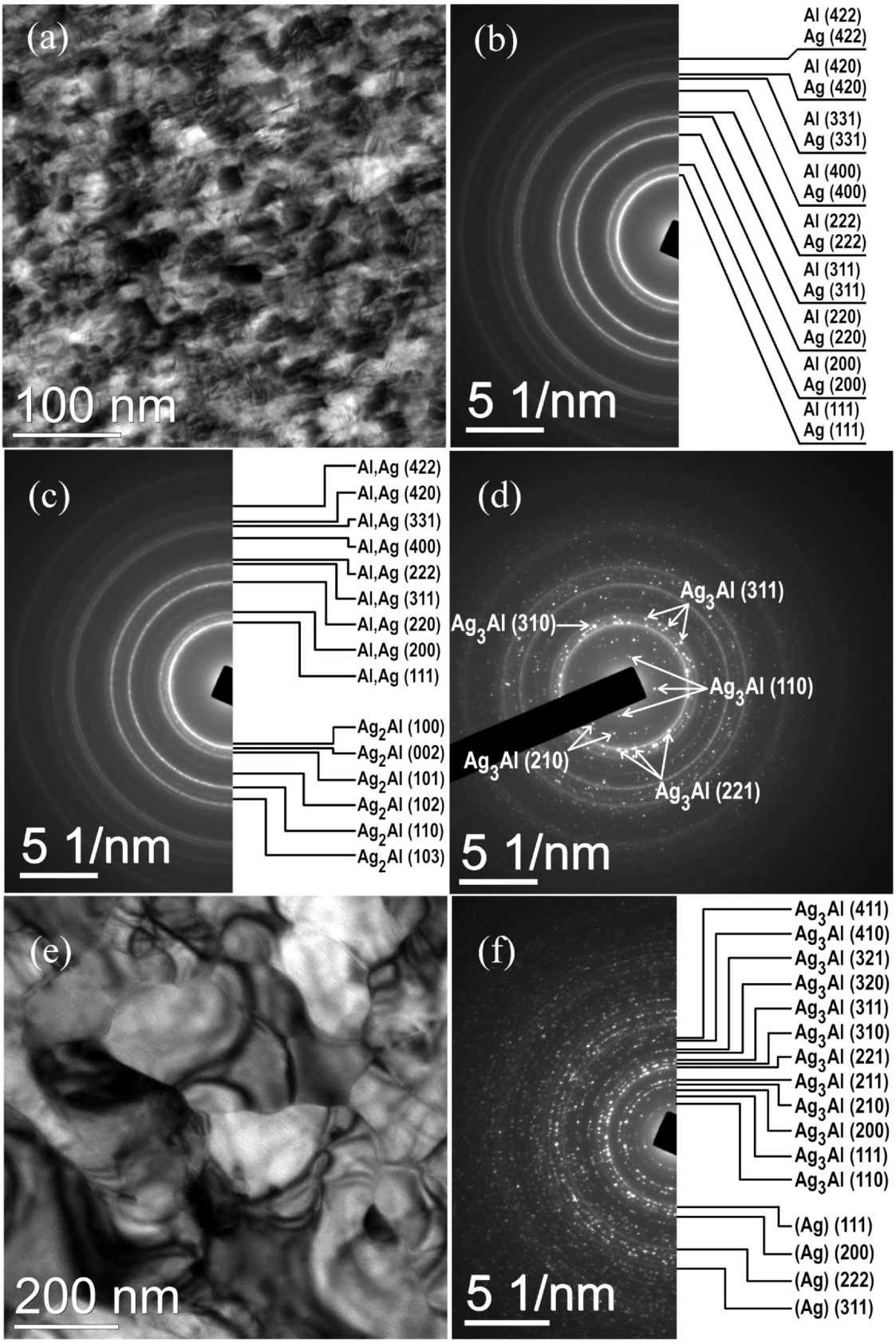

Fig. 1. TEM image (a) and SAED pattern (b) of the Ag/Al film at the initial state. SAED patterns after heating the film to 125 °C (c) and 175 °C (d) at a heating rate of 10 °C/min. TEM image (e) and ED pattern (f) of the film after heating to 300 °C.

crystallites in the Ag/Al films was equal to 10–20 nm. The diffraction reflections observed in the electron diffraction pattern (Fig. 1(b)), correspond to the phases of fcc Ag (PDF 4 + #00-004-0783, Fm-3 m, a = 4.086 Å) and fcc Al (PDF 4 + #00-004-0787, Fm-3 m, a = 4.049 Å). It is worth noting that the crystal lattice parameters for Al and Ag differ by only 0.9%, as a result, the diffraction reflections in the electron diffraction pattern almost overlap.

Fig. 1(c, d, f) presents the electron diffraction patterns obtained from the film at different heating temperatures, 125 °C, 175 °C and 300 °C, correspondingly. Fig. 1(e) shows an electron microscopy image obtained from the film after heating to 300 °C. The transverse size of the crystallites after heating was equal to 200–400 nm (at the film thickness of 100 nm).

In order to be able to analyze the kinetics of the phase formation in the solid-state reaction upon heating the Ag/Al film at different rates dependences were constructed for the changes in the intensities of the characteristic diffraction reflections of the δ-Ag_2Al and μ-Ag_3Al phases depending on the heating temperature (Fig. 2(a, b)).

As a result of analyzing the intensities of the diffraction reflections it was established that upon heating Ag/Al at a rate of 5 °C/min (Fig. 2(a)) upon reaching 93 °C nanocrystallites of the phase δ-Ag_2Al (PDF 4 + #00-014-0647, $P6_3/mmc$, a = 2.885 Å, c = 4.624 Å) appeared on the boundary of the silver and aluminium nanolayers. Upon reaching 142 °C nanocrystallites of the phase μ-Ag_3Al (PDF 4 + #00-026-1330, P4132, a=6.946 Å) began to form. At the increasing heating rate from 5° to 10 °C/min the initial stage of the formation for the phases δ-Ag_2Al and μ-Ag_3Al, was observed to shift, by 4 °C and 8 °C respectively, to the area of higher temperatures (Fig. 2(a,b)). The temperature of the completion of the solid-state reaction between the aluminium and silver nanolayers was also shifted to the range of high temperatures from 233 °C to 242 °C.

Thus, the phase transformation process in the system under study can be presented as the following stages:

$$Ag+Al \rightarrow (Ag)+(Al) \rightarrow (Ag) + \delta\text{-}Ag_2Al \rightarrow \mu\text{-}Ag_3Al.$$

It is known [15,36], that at the initial stage of the solid-state reaction solid solutions of (Ag) and (Al) are formed on the boundary between the phases followed by the precipitation of the δ-Ag_2Al phase from the solid solution of (Al), characterized by a narrower area of homogeneity in the Ag-Al system at T < 300 °C [11]. However, based on the electron diffraction data it is not possible to make a conclusion concerning the formation of the (Ag) and (Al) solid solutions since their characteristic diffraction reflections almost coincide with the reflections of Ag and Al, which makes it impossible to identify the reflections corresponding to the solid solutions.

3.2. DTA-TG investigations

The $(Ag/Al)_{15}$ multilayer films were used for simultaneous thermal analysis experiments Fig. S1(a) presents a STEM image of the cross-section of the $(Ag/Al)_{15}$ film and Fig. S1(b, c) shows the distribution maps of Ag and Al. An X-ray diffraction pattern obtained from the $(Ag/Al)_{15}$ at the initial state is shown in Fig. 3(a). The analysis of the intensities of the diffraction reflections indicated the presence of the predominant orientation of the silver and aluminium crystallites, the planes of the Ag(111) and Al(111) type were parallel to the plane of the substrate. After heating the $(Ag/Al)_{15}$ film to 300 °C only crystallites of the μ-Ag_3Al phase and solid solution based on silver (Ag) were present (see Fig. 3(b)).

The simultaneous thermal analysis of the $(Ag/Al)_{15}$ multilayer sample shows (see Fig. 4), that in the temperature range of 40–300 °C, two pronounced exothermic peaks are observed on the DTA curves (at heating rates of 5, 10 and 20 °C/min). These peaks correspond to the formation processes of the new phases: the low temperature peak - to the formation of the δ-Ag_2Al phase and the high temperature one - to the μ-Ag_3Al phase. The TG curves show slight changes in the mass within 0.07–0.18 wt%, mainly caused by the loss of sorbed water and oxidation of adsorbed organic compounds.

Depending on the heating rate (Table 1) the δ-Ag_2Al phase was observed to form in the range of 98–111 °C, the maximum rate of the phase formation was reached at 113–127 °C, the process finished at 124–143 °C. The formation of the μ-Ag_3Al phase in the high temperature range was characterized by the same parameters: the beginning at 153–173 °C, maximum at 161–183 °C and the process finished at 169–194 °C (Table 1). It is worth noting that with the increase in the heating rate, a better separation of exothermic peaks is observed (see Table 1). As it is shown in [37], this may indicate a higher value of the activation energy for the low-temperature reaction compared to the high-temperature one, which is a characteristic feature only for the two-steps sequential process.

3.2.1. Model-free estimation of the activation energy and multi-step nature of the reaction

The model-free methods of Kissinger [38] and Friedman [39] were used to preliminary estimate the kinetic parameters (apparent activation energy, reaction order and pre-exponential factor) in this study. The first method allows estimating the values of the apparent activation energy based on the data on the location of the peak maxima on the DTA curve at different heating rates and the apparent reaction order can be determined from the temperature parameters related to the asymmetry of the signal peak. The second method

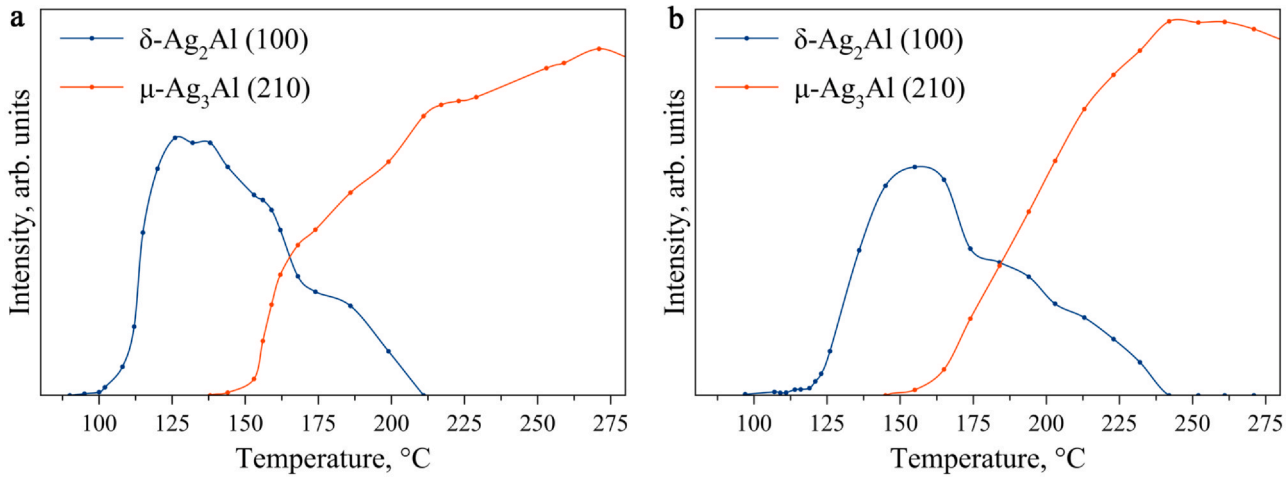

Fig. 2. The variation of the ED reflection intensity during heating Ag/Al at a heating rate of 5 °C/min (a) and 10 °C/min (b).

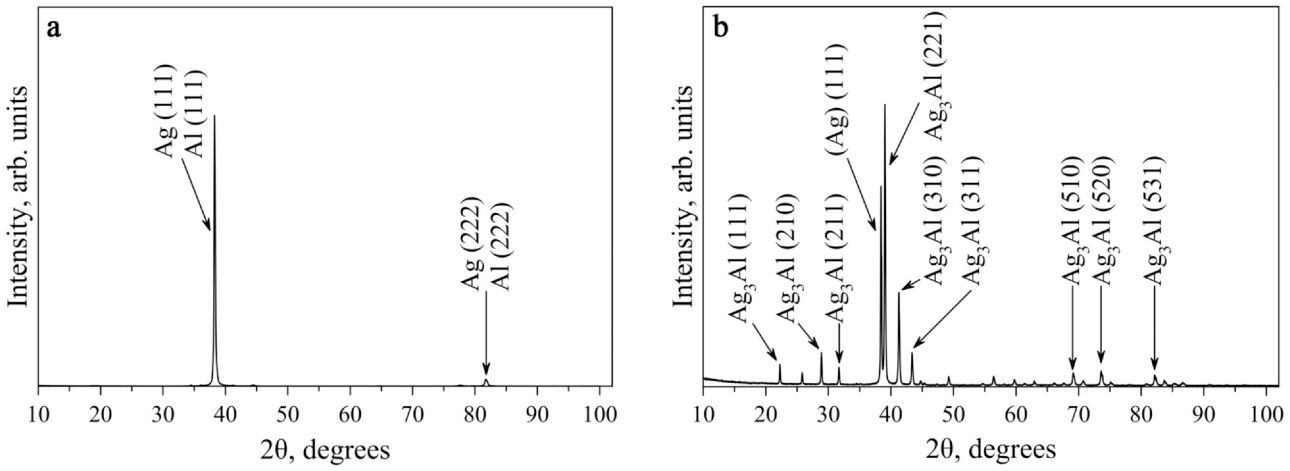

Fig. 3. XRD patterns of the $(Ag/Al)_{15}$ at the initial state (a) and after heating to 300 °C (b).

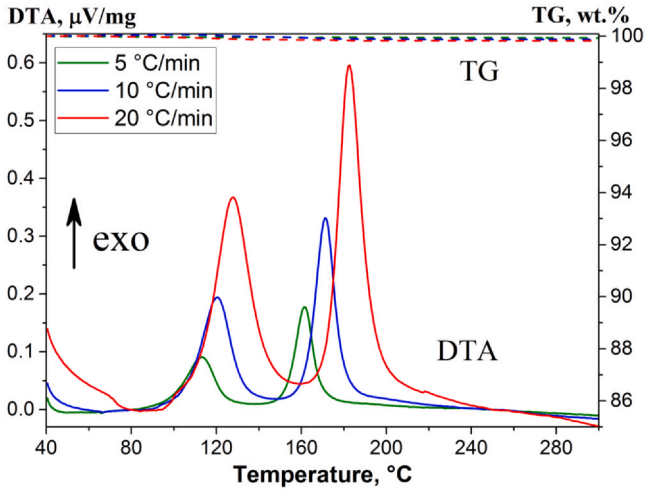

Fig. 4. DTA and TG curves of the multilayer sample $(Ag/Al)_{15}$ at different heating rates: 5, 10 and 20 °C/min.

Table 1
DTA data for the main exothermic peaks of the process of the thermo-chemical transformations in the Al-Ag multilayer system.

Heating rate β, °C/min	DTA data for the low-temperature peak, °C			DTA data for the high-temperature peak, °C		
	T_{onset}	T_{peak}	T_{end}	T_{onset}	T_{peak}	T_{end}
5	98	113	124	153	161	169
10	105	121	133	162	171	180
20	111	127	143	173	183	194

(in this study implemented in the software "Netzsch Thermokinetic 3") allows obtaining the dependence of the apparent activation energy and pre-exponential factor on the rate of conversion of the material from the whole set of the DTA curves recorded at different heating rates, assuming that this is a first-order reaction.

The analysis of the DTA curves using the Kissinger method [38,40] allowed estimating the apparent activation energies and reaction orders (the last one could be estimated based on the asymmetry parameters of the peaks according to the technique [38]) for both steps of the solid-state transformation process (Fig. 5). The basic conditions of the applicability of the Kissinger method are [41]: (i) one-step process, (ii) temperature of the peak maximum of the thermoanalytical curve (in the case of the isoconversional type of this method, namely, the Kissinger-Akahira-Sunose method, at a temperature corresponding to a certain degree of conversion) obtained only in the linear heating; (iii) the reaction order should be close to 1. It is determined that the low-temperature step is characterized by E_a = 112 ± 6 kJ/mol, log(A, 1/sec) = 13 ± 4 and n = 1.1, and the high-temperature step, by, E_a = 96 ± 4 kJ/mol, log(A, 1/sec) = 9 ± 3 and n = 1.3 respectively.

The kinetic analysis based on the Friedman model-free method allows one to prove that the process of solid-state transformations in the $(Ag/Al)_{15}$ multilayer sample is successive and has two steps which is revealed by the presence of two distinct "plateaus" on the curve of the dependence of E_a on the conversion rate (Fig. 6). As in the case of the analysis results according to the Kissinger method, here, the high-temperature step is also characterized by a higher activation energy E_a = 128 ± 1 kJ/mol (the pre-exponential factor log (A, 1/sec) = 14.8 at a conversion rate of α = 0.1), as compared to the low-temperature step – E_a = 97 ± 1 kJ/mol (the pre-exponential factor log(A, 1/sec) = 9.8 at α = 0.65). A considerable increase in the error in determining the apparent activation energy at α < 0.05, α = 0.20–0.55 and α > 0.70 is related to the increasing contribution of the partial diffusion control of the reaction [42], which is not considered in the model-free method. The symbate behavior of the curves of the apparent activation energy and pre-exponential factor is explained by the manifestation of the enthalpy-entropy compensation effect [43].

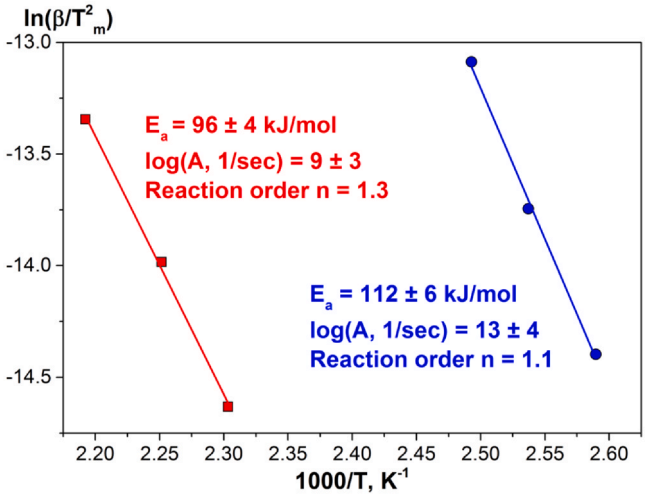

Fig. 5. Kissinger plots for the low- and high-temperature peaks from the DTA data, and calculated kinetic parameters (apparent activation energy, pre-exponential factor and apparent reaction order).

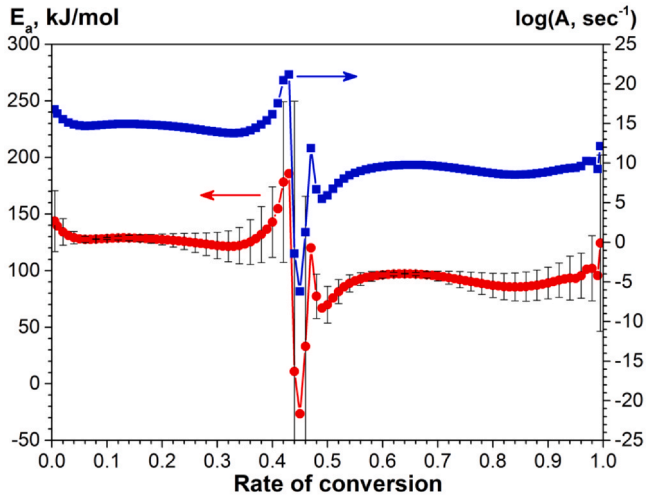

Fig. 6. Activation energy and pre-exponential factor as the functions of conversion from the Friedman model-free analysis of the DTA data.

Thus, the estimates of the kinetic parameters obtained using the model-free methods can be used as the initial conditions in the model description of the observed multi-step process of the solid-state transformation by the method of multivariate non-linear regression [44] using the software package "Netzsch Thermokinetics 3".

3.2.2. Selection of reaction model

The main aspects of the kinetic analysis using the multivariate non-linear regression, as well as the basic equations of kinetics of solid-state reactions are given in [44] and in more detail in [45–47]. Preliminary, the correction of the baseline was made according to the tangential-sigmoid type to decrease the contribution of the temperature dependence for the heat capacity of the phases being formed.

In the process of modeling, the values of the apparent activation energy and pre-exponential factors obtained by the Friedman model-free analysis were used as the initial parameters (see Section 3.2.1). Using the software package "NETZSCH Thermokinetics 3" kinetic parameters were calculated for each step of the successive two-step solid-state transformation with the application of several kinetic models [44]. The degree of conformity in the description of the experimental data was determined using the maximum Pearson correlation coefficient ***r*** and Fisher criterion (the condition $F_{exp} < F_{crit,0.05}$ must be fulfilled at the level of confidence of 0.05).

The models for the two-step process of the solid-state transformation with higher correlation coefficients are given in Table 2: "Cn-X" is the nth order reaction with autocatalysis through the reactants, X (X is a product in the complex model, frequently $X = p$); "Bna" is the expanded Prout–Tompkins equation; "C1-X" is the first-order reaction with autocatalysis through the reactants, X (X is a product in the complex model, frequently $X = p$); "An" is the *n*-dimensional nucleation/nucleus growth according to Avrami-Erofeev; "Fn" is the nth order reaction; "F1" is the first-order reaction; "D3" is three-dimensional diffusion (Jander's type). A detailed mathematical description of these kinetic models is presented in [44].

From Table 2 one can see that, the nth order reaction with autocatalysis is the model which simultaneously meets the Fisher criterion ($F_{exp} = 1.00$, which is lower than $F_{crit,0.05}$) and has a higher correlation coefficient r = 0.9980 (Cn-X, Table 2). For this type of reaction the kinetic equation can be written in the general form [44]:

$$de/dt = -Ae^{n}(1+k_{cat}X)\exp(E_a/RT),$$

where *t* is the time, sec.

T is the temperature, K.

E_a is the apparent activation energy, kJ/mol.

n is the reaction order.

e is the starting concentration of the reactant.

p is the concentration of the final product.

k_{cat} is the rate constant of the reaction with autocatalysis by the product X (the product in the complex model, frequently X = p).

The description of the results for the two-step process of the solid-state transformation in the $(Ag/Al)_{15}$ multilayer sample with the help of the kinetic model "Cn-X" is presented in Fig. 7. Each step of the process is characterized by the kinetic parameters presented in Table 3. Assuming the autocatalytic nature of the solid-state transformations in the Ag-Al system, the authors assume that at the first step of the process, the catalytic action is due to the intermediate product δ-Ag_2Al, and at the second step it is caused by the product μ-Ag_3Al. According to the definition of the kinetic model "Cn-X" [42], the catalytic and non-catalytic routes of each of the steps have the same activation energy and proceed in parallel, and the magnitude of the catalytic action is determined by the reaction rate constant k_{cat}.

The value of the apparent activation energy for the formation process of the phase δ-Ag_2Al (E_a = 112 ± 6 kJ/mol) in the solid-state reaction calculated in this study by the Kissinger method for the $(Ag/Al)_{15}$ multilayer system with the bilayer thickness equal to 100 nm is in good agreement with the data in [22] – 111–125 kJ/mol, where the calculation was made by the same method. Also, good coincidence with E_a = 110 kJ/mol, measured in the isothermal mode taking into account the rate of the changing thickness of the δ-Ag_2Al phase being formed, was demonstrated in [23] for Ag/Al bilayer films with the thickness of 300–700 nm. However, in [24] it is shown that the apparent activation energy of the formation for the δ-Ag_2Al phase of Ag/Al bilayer films with the thickness of 460 nm Al - 270 nm, Ag - 190 nm) was equal to 83 kJ/mol. The lower value of the apparent activation energy is explained by the contribution of diffusion along the grain boundaries (or surface diffusion) into the formation rate of δ-Ag_2Al, moreover, with the increasing layer thickness (of the diffusion area) of this phase the diffusion on the grain boundary becomes a limiting process. In this study, the values of the kinetic parameters for the δ-Ag_2Al phase formation process were specified (see Table 3), using the model description of the solid-state interaction in the Ag-Al system, in particular, the apparent activation energy was 126 kJ/mol.

Further, in this study, for the formation process of the μ-Ag_3Al phase in the nanolayer sample, for the first time apparent kinetic parameters of the Arrhenius dependence were obtained, as well as the reaction order and the rate constant of the autocatalytic reaction (see Table 3) The apparent activation energy for the formation of μ-Ag_3Al is slightly lower (106.2 kJ/mol) as compared to E_a in the case of the δ-Ag_2Al phase (126.0 kJ/mol), which is in the frames of the activated complex theory (proportional relationship between E_a and enthalpy of formation) and is in good agreement with the respective enthalpy values ΔH` for the formation of these phases (taken in absolute value) [25]: |− 3.12 kJ/mol| and |− 4.09 kJ/mol|, respectively.

Besides, it is worth noting that the process of solid-state transformation under study is well described by the expanded Prout-Tompkins equation ("Bna", Table 2), which, in its turn is a special case of the Sestak-Berggren's equation, which also describes an autocatalytic process [45].

Fig. 8 presents the kinetic curves of the solid-state transformations describing the changes in the content of the crystalline phases δ-Ag_2Al and μ-Ag_3Al in the process of linear heating (at 5 °C/min and 10 °C/min) of the $(Ag/Al)_{15}$ multilayer sample. The curves are built based on the results of the model description for the DTA thermal analysis data which correspond to the two-step autocatalytic process (Cn-X). The analysis shows that these kinetic curves are in good

Table 2
Results of the multiple-curve analysis of the thermal transformations in the $(Ag/Al)_{15}$ multilayer sample, measured at heating rates of 5, 10 and 20 °C/min.

Reaction type [44]	E_a, kJ/mol		log (A, s^{-1})		Corr. coeff.	F-test	
	Step 1	Step 2	Step 1	Step 2		F_{exp}	$F_{crit\ (0.05)}$
Cn-X	126.0	106.2	14.65	8.82	0.9980	1.00	1.11
Bna	125.7	106.2	15.19	11.27	0.9976	1.20	1.11
C1-X	124.0	104.7	14.52	9.18	0.9885	6.22	1.11
An	124.1	105.1	14.71	10.39	0.9827	9.25	1.11
Fn	150.3	133.4	18.25	13.69	0.8926	53.38	1.11
F1	154.2	197.7	18.77	21.36	0.8781	58.72	1.11
D3	240.3	317.8	29.21	34.34	0.8091	87.88	1.11

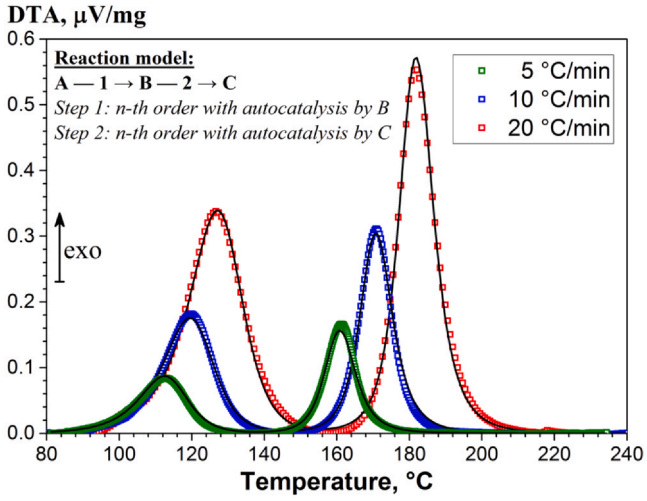

Fig. 7. Kinetic analysis of the DTA measurements of the $(Ag/Al)_{15}$ multilayer sample with the best fit of the reaction type Cn-X (nth order reaction with autocatalysis) for each step. Squares – measured, lines – calculated.

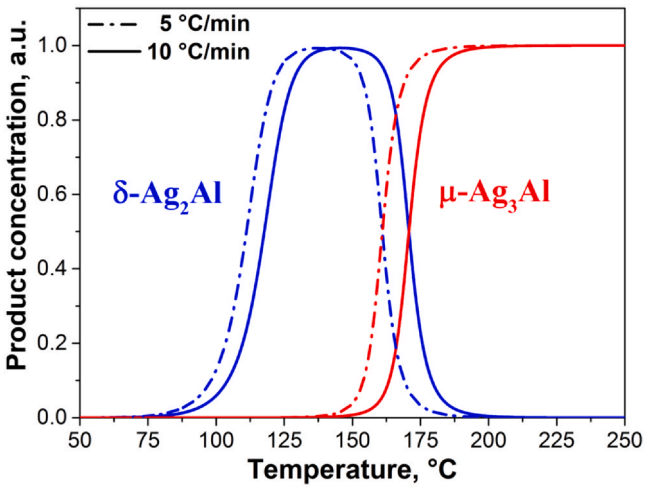

Fig. 8. Kinetic curves for the phase transformation in the Ag-Al system according to the results of prediction based on the thermokinetic best fit of the DTA data: heating rate of 5 °C/min (dash dot lines) and 10 °C/min (solid lines).

Table 3
Apparent activation energy, pre-exponential factor, reaction order and autocatalysis rate constant of the reaction type "Cn-X" for each step.

Kinetic parameters	Step 1: formation of *δ-Ag_2Al*	Step 2: formation of *μ-Ag_3Al*
E_a, kJ/mol	126.0	106.2
log (A, 1/sec)	14.65	8.82
n	1.45	1.56
log (k_{cat})	0.69	2.55

agreement with the experimental data given in Fig. 2(a,b) which presents the curves of changes in the intensity of the diffraction reflections for the phases δ-Ag_2Al and μ-Ag_3Al in the solid-state reaction process at a heating rate of 5 °C/min and 10 °C/min of the Ag/Al bilayer sample. A rather good coincidence is observed for the starting temperatures of the formation of the crystalline phases δ-Ag_2Al and μ-Ag_3Al. The disagreement in the range of the beginning of the solid-state reaction at the heating rate of 5 °C/min, corresponding to 78 °C (Fig. 8) on the model curve and to 93 °C on the experimental curve (Fig. 2(a)), is explained by the fact that the solid-state reaction begins with the formation of the solid solution of Ag-Al, which cannot be identified by the electron diffraction method. The disagreement of the temperature range for the existence of the δ-Ag_2Al – phase: to 187 °C (Fig. 8) and to 210 °C (Fig. 2(a)) can be explained by the fact that the model curves (see Fig. 8) are built based on the analysis of the solid-state reaction in the $(Ag/Al)_{15}$, multilayer system, however the experimental data (see Fig. 2(a, b)) are obtained in the Ag/Al bilayer system. The thicknesses of the individual silver and aluminium nanolayers as well as the crystallite sizes coincide in the cases of the bilayer and multilayer systems. However, in the bilayer system there is only one interface where the diffusion of the reacting elements occurs. In the multilayer system each nanolayer has two interfaces, thus the effective diffusion value proves to be higher.

4. Conclusions

The main conclusions are the following:

1) A detailed kinetic analysis was made of the phase formation processes in the solid-state reaction in the Ag/Al nanosized multilayer system within a wide temperature range of 40–300 °C.
2) The process of solid-state interaction in the Ag-Al system is shown to consist of two-steps. Each step can be described by the kinetic model of the n^{th} order autocatalytic reactions with the high level of confidence (R = 0.9980).
3) Based on the data obtained by the methods of *in situ* electron diffraction and simultaneous thermal analysis it was shown that the low-temperature step corresponded to the formation of the δ-Ag_2Al phase and was characterized by the apparent activation energy E_a = 126 kJ/mol, reaction order n = 1.45 and pre-exponential factor log(A, 1/sec) = 14.65. At the high-temperature

step the μ-Ag_3Al phase was formed, whose kinetic parameters were determined to be: E_a = 106 kJ/mol, n = 1.56 and log(A, 1/sec) = 8.82.

4) It was shown that the phase transformation process in the Ag/Al multilayer system (the atomic ratio Ag:Al=80:20) could be presented by the following stages:

$$Ag + Al \rightarrow (Ag) + (Al) \rightarrow (Ag) + \delta\text{-}Ag_2Al \rightarrow \mu\text{-}Ag_3Al.$$

CRediT authorship contribution statement

Sergey M. Zharkov: Conceptualization, Investigation, Writing - review & editing, Supervision, Project administration, Funding acquisition. **Roman R. Altunin:** Investigation, Formal analysis, Visualization. **Vladimir V. Yumashev:** Methodology, Formal analysis, Investigation, Writing - original draft, Visualization. **Evgeny T. Moiseenko:** Methodology, Formal analysis, Visualization. **Oleg V. Belousov:** Writing - review & editing. **Leonid A. Solovyov:** Formal analysis, Investigation. **Mikhail N. Volochaev:** Investigation. **Galina M. Zeer:** Investigation.

Data availability statement

The datasets generated and analyzed during the current study are available from the corresponding authors on reasonable request.

Funding

This work was supported by the Russian Science Foundation, Russia under grant #18-13-00080.

Declaration of Competing Interest

The authors declare that they have no known competing financial interests or personal relationships that could have appeared to influence the work reported in this paper.

Acknowledgements

The TEM cross-section specimens were prepared by the FIB technique in the Krasnoyarsk Regional Center of Research Equipment of Federal Research Center "Krasnoyarsk Science Center SB RAS". The electron microscopy investigations were conducted in the SFU Joint Scientific Center whose infrastructure was supported by the State assignment (#FSRZ-2020-0011) of the Ministry of Science and Higher Education of the Russian Federation.

Appendix A. Supporting information

Supplementary data associated with this article can be found in the online version at doi:10.1016/j.jallcom.2021.159474.

References

[1] D. Gu, Ch Zhang, Yi-K. Wu, L.J. Guo, Ultra-smooth and thermally-stable Ag-based thin with subnanometer roughness by Al doping, ACS Nano 8 (2014) 10343–10351, https://doi.org/10.1021/nn503577c
[2] K.S.B. De Silva, V.J. Keast, A. Gentle, M.B. Cortie, Optical properties and oxidation of α-phase Ag–Al thin films, Nanotechnology 28 (2017) 095202–095210, https://doi.org/10.1088/1361-6528/aa5782
[3] J.H. Im, K.-T. Kang, S.H. Lee, J.Y. Hwang, H. Kang, Bulk-like Al/Ag bilayer film due to suppression of surface plasmon resonance for high transparent organic LEDs, Org. Electron. 33 (2016) 116–120, https://doi.org/10.1016/j.orgel.2016.03.002
[4] M. Qian, X.B. Shi, J. Ma, J. Liang, Y. Liu, Zh-K. Wang, L.-Sh Liao, A stacked Al/Ag anode for short circuit protection in ITO free top-emitting organic light-emitting diodes, RCS Adv. 5 (2015) 96478–96482, https://doi.org/10.1039/C5RA18132A
[5] M.-G. Song, K.-S. Kim, H.I. Yang, J.-H. Kim, Ch-W. Han, H.-Ch Choi, R. Pode, J.H. Kwon, Highly reliable and transparent Al doped Ag cathode fabricated using thermal evaporation for transparent OLED applications, 105418-105418, Org. Electron. 76 (2020) 105418, https://doi.org/10.1016/j.orgel.2019.105418
[6] M.K.M. Ali, K. Ibrahim, E.M. Mkawi, Ag-Al alloy thin film on plastic substrate by screen printing for solar cell back contact application, Mater. Sci. Semicond. Process. 16 (2013) 593–597, https://doi.org/10.1016/j.mssp.2012.10.006
[7] L. Liang, Z.G. Li, L.K. Cheng, N. Takeda, A.F. Carroll, Microstructural characterization and current conduction mechanisms of front-side contact of n-type crystalline Si solar cells with Ag/Al pastes, J. Appl. Phys. 117 (2015) 215102–215107, https://doi.org/10.1063/1.4921544
[8] Y. Chen, L. Wen, X. Hu, R. Xu, Q. Chen, Discrete optical field manipulation by Ag-Al bilayer gratings for broadband absorption enhancement in thin-film solar cells, Plasmonics 13 (2018) 1603–1613, https://doi.org/10.1007/s11468-017-0669-z
[9] Y.N. Zhou (Ed.), Microjoining and nanojoining, Woodhead Publishing, Cambridge, 2008ISBN: 9781845691790.
[10] D.J. Fisher, Bonding by self-propagating reaction, Materials Research Forum LLC, Millersville, PA, 2019 ISBN: 978-1-64490-008-6.
[11] T.B. Massalski, H. Okamoto, P.R. Subramanian, L. Kacprzak (Eds.), Binary Alloy Phase Diagrams //, 2nd ed., ASM International, Materials Park. Ohio, 1990, p. 3589 ISBN: 978-0-87170-403-0.
[12] B. Predel, O. Madelung (Eds.), Phase Equilibria, Crystallographic and Thermodynamic Data of Binary Alloys, Landolt-Börnstein - Group IV Physical Chemistry, Vol. 5A Springer, Ag-Al (Silver-Aluminum), 1991, , https://doi.org/10.1007/10000866_9
[13] L.F. Mondolfo, Aluminum Alloys. Structure and Properties, Butterworth & Co Publishers Ltd., 1976, pp. 213–224, https://doi.org/10.1016/B978-0-408-70932-3.50015-2
[14] N.A. Zarkevich, D.D. Johnson, Predicted hcp Ag-Al metastable phase diagram, equilibrium ground states, and precipitate structure, Phys. Rev. B 67 (2003) 064104–064108, https://doi.org/10.1103/PhysRevB.67.064104
[15] S.-W. Fu, Ch.C. Lee, A study on intermetallic compound formation in Ag-Al system and evaluation of its mechanical properties by micro-indentation, J. Mater. Sci. Mater. Electron. 29 (2018) 3985–3991, https://doi.org/10.1007/s10854-017-8340-1
[16] S.-W. Fu, Ch.C. Lee, New solid-state die-attach method using Ag foil bonded on Al substrate by eutectic reaction, J. Alloy. Compd. 774 (2019) 1207–1215, https://doi.org/10.1016/j.jallcom.2018.09.254
[17] M. Schneider-Ramelow, Ch Ehrhardt, The reliability of wire bonding using Ag and Al, Microelectron. Reliab. 63 (2016) 336–341, https://doi.org/10.1016/j.microrel.2016.05.009
[18] M.-R. Choi, H.-G. Kim, T.-W. Lee, Y.-J. Jeon, Y.-K. Ahn, K.-W. Koo, Y.-Ch Jang, S.-Y. Park, J.-H. Yee, N.-K. Cho, I.-T. Kang, S. Kim, S.-Z. Han, S.-H. Lim, Microstructural evaluation and failure analysis of Ag wire bonded to Al pads, Microelectron. Reliab. 55 (2015) 2306–2315, https://doi.org/10.1016/j.microrel.2015.07.038
[19] J. Wu, Y. Huo, Ch.C. Lee, Complete elimination of Ag_3Al in Ag wire bonds on Al by alloying In into Ag', Materialia 2 (2018) 82–97, https://doi.org/10.1016/j.mtla.2018.06.013
[20] D.P. Adams, Reactive multilayers fabricated by vapor deposition: a critical review, Thin Solid Films 576 (2015) 98–128, https://doi.org/10.1016/j.tsf.2014.09.042
[21] A.S. Rogachev, S.G. Vadchenko, A.S. Mukasyan, Self-sustained waves of exothermic dissolution in reactive multilayer nano-foils, 063119-4, Appl. Phys. Lett. 101 (2012) 063119, https://doi.org/10.1063/1.4745201
[22] H. Aboulfadl, I. Gallino, R. Busch, F. Mücklich, Atomic scale analysis of phase formation and diffusion kinetics in Ag/Al multilayer thin films, J. Appl. Phys. 120 (2016) 195306–195313, https://doi.org/10.1063/1.4968013
[23] C. Weaver, L.C. Brown, Diffusion in evaporated films of silver–aluminium, Philos. Mag. 17 (1968) 881–897, https://doi.org/10.1080/14786436808223171
[24] J.E.E. Baglin, F.M. d'Heurle, W.N. Hammer, The interaction process for Ag-Al polycrystalline thin-film couples, J. Appl. Phys. 50 (1979) 266–275, https://doi.org/10.1063/1.325710
[25] R.R. Altunin, E.T. Moiseenko, S.M. Zharkov, Effect of the structural properties on the electrical resistivity of the Al/Ag thin films during the solid-state reaction, Phys. Solid State 62 (2020) 621–626, https://doi.org/10.1134/S1063783420040034
[26] Powder Diffraction File (PDF 4+, 2020), Inorganic Phases Database, International Center for Diffraction Data (ICDD), Swarthmore, PA, USA. http://www.icdd.com/products/pdf4.htm.
[27] P. Villars, K. Cenzual, Pearson's Crystal Data: Crystal Structure Database for Inorganic Compounds (on CD-ROM), Release 2011/12, ASM International®, Materials Park, Ohio, USA.
[28] E.T. Moiseenko, R.R. Altunin, S.M. Zharkov, *In situ* electron diffraction and resistivity characterization of solid-state reaction process in Cu/Al bilayer thin films, Metall. Mater. Trans. A 51 (2020) 1428–1436, https://doi.org/10.1007/s11661-019-05602-5
[29] E.T. Moiseenko, S.M. Zharkov, R.R. Altunin, O.V. Belousov, L.A. Solovyov, V.V. Yumashev, M.N. Volochaev, G.M. Zeer, Peculiarities of intermetallic phase formation in the process of a solid state reaction in $(Al/Cu)_n$ multilayer thin films, JOM 73 (2021) 580–588, https://doi.org/10.1007/s11837-020-04522-9
[30] R.R. Altunin, E.T. Moiseenko, S.M. Zharkov, Structural phase transformations in Al/Pt bilayer thin films during the solid-state reaction, Phys. Solid State 60 (2018) 1413–1418, https://doi.org/10.1134/S106378341807003X
[31] S.M. Zharkov, E.T. Moiseenko, R.R. Altunin, $L1_0$ ordered phase formation at solid-state reactions in Cu/Au and Fe/Pd thin films, J. Solid State Chem. 269 (2019) 36–42, https://doi.org/10.1016/j.jssc.2018.09.009

[32] R.R. Altunin, E.T. Moiseenko, S.M. Zharkov, Structural phase transformations during a solid-state reaction in a bilayer Al/Fe thin-film nanosystem, Phys. Solid State 62 (2020) 200–205, https://doi.org/10.1134/S1063783420010059
[33] S.M. Zharkov, R.R. Altunin, E.T. Moiseenko, G.M. Zeer, S.N. Varnakov, S.G. Ovchinnikov, Solid-state reactions in Fe/Si multilayer nanofilms, Solid State Phenom. 215 (2014) 144–149, https://doi.org/10.4028/www.scientific.net/SSP.215.144
[34] S.M. Zharkov, E.T. Moiseenko, R.R. Altunin, N.S. Nikolaeva, V.S. Zhigalov, V.G. Myagkov, Study of solid-state reactions and order-disorder transitions in Pd/α-Fe(001) thin films, JETP Lett. 99 (2014) 405–409, https://doi.org/10.1134/S0021364014070145
[35] E.T. Moiseenko, R.R. Altunin, S.M. Zharkov, Formation of the atomically ordered $L1_0$ structure with the [001] orientation during the solid-state reaction in Fe/Pd bilayer thin films, Phys. Solid State 59 (2017) 1233–1237, https://doi.org/10.1134/S1063783417060154
[36] S.-W. Fu, C.C. Lee, Direct silver to aluminum solid-state bonding processes, Mater. Sci. Eng. A 722 (2018) 160–166, https://doi.org/10.1016/j.msea.2018.03.011
[37] M. Edelmann, G. Heinrich, Thermokinetic analysis of two-step curing reactions in melt: Part II. Investigation of polymeric model systems, Thermochim. Acta 499 (2010) 160–165, https://doi.org/10.1016/j.tca.2009.12.006
[38] H.E. Kissinger, Reaction kinetics in differential thermal analysis, Anal. Chem. 29 (1957) 1702–1706, https://doi.org/10.1021/ac60131a045
[39] H.L. Friedman, Kinetics of thermal degradation of char-forming plastics from thermogravimetry. application to a phenolic plastic, J. Polym. Sci. Part C. 6 (1964) 183–195, https://doi.org/10.1002/polc.5070060121
[40] ASTM E2890–12^{e1}. Standard test method for kinetic parameters for thermally unstable materials by differential scanning calorimetry using the Kissinger method. DOI: 10.1520/E2890–12E01.
[41] S. Vyazovkin, Kissinger method in kinetics of materials: things to beware and be aware of, Molecules 25 (2020) 2813, https://doi.org/10.3390/molecules25122813
[42] J.R. Opfermann, E. Kaisersberger, H.J. Flammerssheim, Model-free analysis of thermoanalytical data – advantages and limitations, Thermochim. Acta 391 (2002) 119–127, https://doi.org/10.1016/S0040-6031(02)00169-7
[43] B.V. L'vov, A.K. Galwey, Interpretation of the kinetic compensation effect in heterogeneous reactions: thermochemical approach, Int. Rev. Phys. Chem. 32 (2013) 515–557, https://doi.org/10.1080/0144235X.2013.802109
[44] J. Opfermann, Kinetic analysis using multivariate non-linear regression. I. Basic concepts, J. Therm. Anal. Calorim. 60 (2000) 641–658, https://doi.org/10.1023/A:1010167626551
[45] S. Vyazovkin, A.K. Burnham, J.M. Criado, L.A. Pérez-Maqueda, C. Popescu, N. Sbirrazzuoli, ICTAC Kinetics Committee recommendations for performing kinetic computations on thermal analysis data, Thermochim. Acta 520 (2011) 1–19, https://doi.org/10.1016/j.tca.2011.03.034
[46] E. Moukhina, Determination of kinetic mechanisms for reactions measured with thermoanalytical instruments, J. Therm. Anal. Calorim. 109 (2012) 1203–1214, https://doi.org/10.1007/s10973-012-2406-3
[47] S. Vyazovkin, A.K. Burnham, L. Favergeon, N. Koga, E. Moukhina, L.A. Pérez-Maqueda, N. Sbirrazzuoli, ICTAC kinetics committee recommendations for analysis of multi-step kinetics, Thermochim. Acta 689 (2020) 178597, https://doi.org/10.1016/j.tca.2020.178597